

Weighted Mean Frequencies: a handcraft Fourier feature for 4D Flow MRI segmentation

Simon Perrin¹[0009-0005-2008-2802], Sébastien Levilly¹[0000-0002-2704-0315],
Huajun Sun², Harold Mouchère¹[0000-0001-6220-7216], and Jean-Michel
Serfaty³[0000-0001-8801-1414]

¹ Nantes Université, École Centrale Nantes, CNRS, LS2N, UMR 6004, F-44000
Nantes, France

{simon.perrin,sebastien.levilly,harold.mouchere}@univ-nantes.fr

² Nantes Université, CHU Nantes, INSERM, CNRS, CRCI2NA, F-44000 Nantes,
France

huajun.sun@chu-nantes.fr

³ CHU Nantes, CNRS, INSERM, L'Institut du Thorax, Nantes Université, 44000
Nantes, France

jeanmichel.serfaty@chu-nantes.fr

Abstract. In recent decades, the use of 4D Flow MRI images has enabled the quantification of velocity fields within a volume of interest and along the cardiac cycle. However, the lack of resolution and the presence of noise in these biomarkers are significant issues. As indicated by recent studies, it appears that biomarkers such as wall shear stress are particularly impacted by the poor resolution of vessel segmentation. The Phase Contrast Magnetic Resonance Angiography (PC-MRA) is the state-of-the-art method to facilitate segmentation. The objective of this work is to introduce a new handcraft feature that provides a novel visualisation of 4D Flow MRI images, which is useful in the segmentation task. This feature, termed Weighted Mean Frequencies (WMF), is capable of revealing the region in three dimensions where a voxel has been passed by pulsatile flow. Indeed, this feature is representative of the hull of all pulsatile velocity voxels. The value of the feature under discussion is illustrated by two experiments. The experiments involved segmenting 4D Flow MRI images using optimal thresholding and deep learning methods. The results obtained demonstrate a substantial enhancement in terms of IoU and Dice, with a respective increase of 0.12 and 0.13 in comparison with the PC-MRA feature, as evidenced by the deep learning task. This feature has the potential to yield valuable insights that could inform future segmentation processes in other vascular regions, such as the heart or the brain.

Keywords: 4D Flow MRI · Handcraft Feature · Segmentation.

1 Introduction

4D Flow MRI is a promising sequence that provides the anatomy and velocity field in a 3D volume and along the cardiac cycle [11]. The quantification of hemo-

dynamic biomarkers, such as wall shear stress (WSS), is enabled by these 3D measurements [7]. The necessity of vessel segmentation for parietal biomarkers, such as WSS, is a source of considerable time loss for clinicians. Nevertheless, state-of-the-art deep-learning approaches have been successfully employed to address this task for specific vessels or organs, necessitating a substantial annotated dataset [1, 3, 10].

Clinicians and state-of-the-art solutions frequently use a handcrafted feature, designated Phase-Contrast Magnetic Resonance Angiography (PC-MRA), which facilitates the distinction between flows, vessels and cavities [4, 5]. The PC-MRA image is the result of the anatomical image and the norm of the velocity field multiplication. Its calculation is possible for each time frame; however, its application is frequently focused on the systolic time. Indeed, diastolic PC-MRA does not benefit from high velocity field and is then degraded by noise. Furthermore, the absence of contrast between the lumen and the background can have a substantial impact on the PC-MRA image [2]. Segmentation of the diastolic period is consequently a challenging issue.

The objective of this study is to propose a new handcraft feature, Weighted Mean Frequencies (WMF), that assists with the segmentation task, whether performed manually or automatically. As outlined in Sec. 2, the purpose of this feature is to depict voxel-wise the predominant blood flow frequencies in a 3D volume. Consequently, WMF is capable of discerning voxels that have experienced pulsatile flow during a specific phase of the cardiac cycle. In order to demonstrate the practical benefits of WMF, a comprehensive investigation into two segmentation tasks is presented in Sec. 3 and 4. The first of these is a threshold segmentation task, and the second is a deep-learning-based segmentation task. In conclusion, the results are discussed in relation to the PC-MRA images.

2 Weighted Mean Frequencies

Weighted Mean Frequencies (WMF) are computed as the mean of the energy-weighted frequencies of the temporal Fourier Transform (FT). Firstly, the FT energies vector $E(u_j)$ is defined as, $|FT(u_j)|^2$, where u_j is a velocity component at the j -th voxel position. Moreover, WMF is calculated by averaging strictly positive frequencies weighted by their energies, as

$$WMF(u_j) = \frac{\sum_{i=1}^n E_i(u_j) f_i}{\sum_{i=1}^n E_i(u_j)}, \quad (1)$$

where f_i is the i -th frequency and n is the number of strictly positive frequencies.

In the following, WMF will represent the 3D volume of the most contributing frequency at voxel level. Since WMF can be computed per component, the goal is to merge them into a single feature representing overall fluid pulsatility energy. A high WMF frequency is observed to reflect increased noise contribution. Therefore, the minimum operator is applied over the WMF for each component:

$$WMF_{\min} = \min(WMF_u, WMF_v, WMF_w), \quad (2)$$

where WMF_{\min} is the minimum WMF of the velocity components (u, v, w).

In order to illustrate the behaviour of the proposed feature on 4D Flow MRI, Figure 1 presents the anatomy, WMF of each component, WMF_{\min} and observation graphs. Figure 1a shows the anatomy of a patient with 4 points located on different region of interest. Figure 1b is the WMF applied on the foot-head velocity component and illustrates perfectly the blood pulse in the ascending and descending aorta. In contrast, WMF_u values increases significantly at the top of the aortic arch. This is a consequence of the absence of velocity in the foot-head direction at this particular location. The same observation applies to the two figures 1c and 1d with, respectively, the left-right and anterior-posterior velocity components. Therefore, the application of the minimum operator in Eq. 2 facilitates the extraction of the most relevant regions from each WMF image. Due to the Fourier Transform operation, WMF is not a temporal feature. The proposed feature provides a representation of the voxels which have been exposed to pulsatile flows.

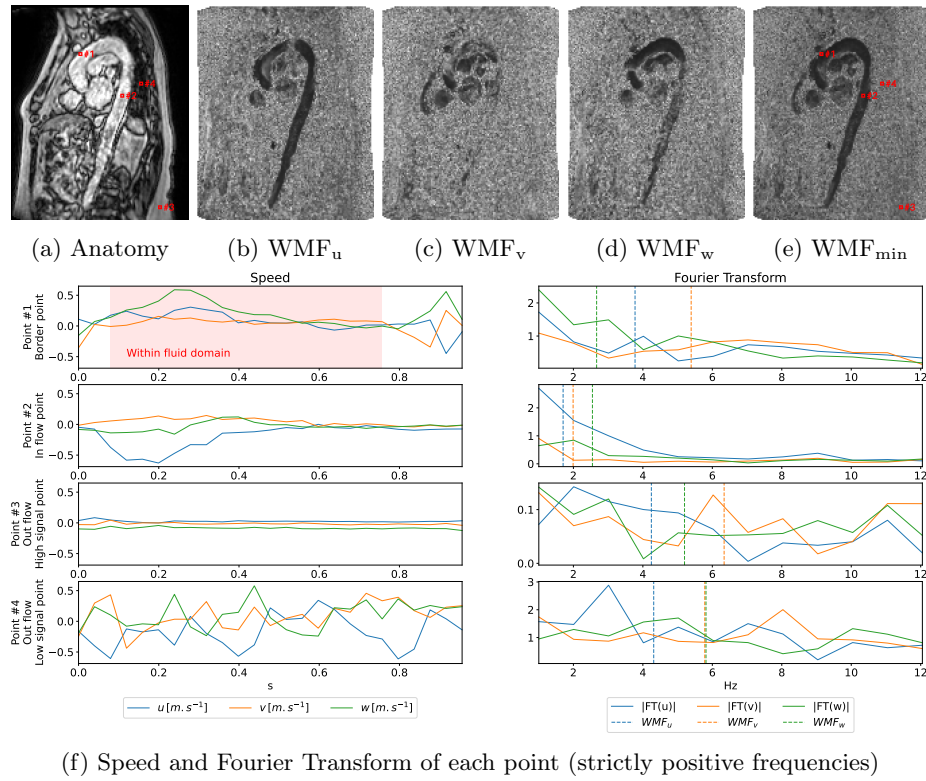


Fig. 1: Images (a) shows the anatomy, (b), (c) and (d) represent the result of WMF for each phase component, (e) is the image obtained using WMF_{\min} and (f) is speed and Fourier Transform analysis at different point in a 4D Flow MRI.

To further investigate WMF feature, Figure 1f presents the temporal evolution of speed and its Fourier Transform for 4 points of interest located in Figure 1a and 1e. Point #1 is located at the border of the aorta. It remains within the aorta and the fluid domain for 17 time frames (illustrated in red on the chart), and subsequently transitions to the exterior domain for the remainder of the time frame. The speed dynamic reveals a distinct change with a smooth evolution during the period in the fluid domain and unstable velocity measurements outside. The resulting FT illustrates the higher pulsatility contribution of the w -velocity component along with its WMF_w . A similar observation can be done for the point #2 which is positioned in the center of the descending aorta. Minor distortions observed in the higher frequencies plateau are attributable to the MRI noise. It results on a small value for WMF which is characteristic of the behaviour of the fluid zone.

The two last points are located fully outside of the fluid domain. Point #3 is taken in a high anatomical signal area in the posterior region that results in a low velocity and low noise [12]. In contrast, Point #4 is located in the lung, exhibiting a weak anatomical signal and therefore high velocity noise. In both situations, the FT displays an absence of a high energy peak in low frequencies, resulting in a high WMF.

Ultimately, the proposed feature associates low frequencies with the fluid domain and with voxels that exhibit intermittent pulsating flow. Finally, the non-fluid domain has been found to contain the highest WMF values, irrespective of the presence of a significant signal in the anatomical image.

For the sake of simplicity, the term WMF is substituted for the term WMF_{\min} in the following sections.

3 WMF in threshold segmentation task

3.1 Method

In order to evaluate the efficacy of WMF in facilitating the segmentation process, a threshold segmentation task is conducted. In this experiment, a comparative analysis is performed on WMF, PCMRA, and combinations of these features in relation to this task. For each MRI in the dataset and each combination, the threshold is optimised by seeking the best intersection over union (IoU) between the ground truth and the resulting segmentation. All features are standardised between 0 and 1, and the threshold is iterated over this range with a step size of 0.02. The application of the threshold is determined by the following criteria: a voxel is classified as true if its value is greater than the threshold. Since WMF assigns a lower value to fluid zones and a higher value to non-fluid zones, the inverse of WMF will be employed here, *i.e.* $1 - \text{WMF}$. In order to establish a comparison between the contributions of WMF and PCMRA to the task, combinations of the two features with anatomy were tested.

Dataset The 4D Flow MRI dataset is based on a retrospective study that includes 43 patients who have experienced a cardiovascular event. The research

was carried out following the principles of the Declaration of Helsinki. The whole dataset is dedicated to the segmentation task of the aorta and has been labeled by non-expert researchers. Labelling has been performed using ITK-SNAP (v4.2.2) [16]. Each MRI is annotated at three distinct time frames: one corresponding to the systolic peak and two frames captured during the diastolic phase, one in the middle of the sequence and the other at the end. The present dataset includes 26 isotropic (ISO) images in addition to 17 non-isotropic images, with spatial resolutions ranging from 2.5 mm to 3 mm. The dataset is separated in 35 1.5 T acquisitions and 8 ones with a 3T magnetic field. Velocity encoding (VENC) changes within the range of 1.5 to $6.0 \text{ m} \cdot \text{s}^{-1}$ across the dataset. This dataset is composed of images acquired in different acquisition planes with various contrast enhancement conditions. The heterogeneity of this dataset is then representative of the clinical condition of acquisition.

Evaluation and Implementation The following evaluation metrics have been selected for the segmentation task: Intersection over Union (IoU), Dice Score, recall and precision. As it is not a learning task, the evaluation is performed on the whole dataset. To compare WMF with PC-MRA, the implementation from Bustamante et al. (2018) [4] has been selected, with a gamma of 0.2 that has been shown to improve the visibility of low velocities. The peak systolic PC-MRA is, due to the high velocity of this frame, the PC-MRA frame where the fluid domain is the most visible. As WMF is not a time-dependent feature, the proposed analysis integrates the use of the systolic PC-MRA, denoted PC-MRA (sys), across all the time frames. Classical PC-MRA computed on each time frame separately is denoted PC-MRA(t) and Mag(t) denotes the anatomical image at the time frame t .

3.2 Results

As demonstrated in Table 1, most of the WMF-derived features manifest better performance on the different metrics than PC-MRA only thresholding. Out of all the possible combinations, WMF is actually the one that exhibits the best performance. Indeed, IoU and Dice Score are higher by 0.025 and 0.034, respectively, compared to the second best method (7th). Compared to the state-of-the-art PC-MRA(t) method, the WMF-based solution achieves improvements in IoU and Dice Score by factors of 2 and 1.9, respectively. The recall is more or less uniform across all features, ranging between 0.555 and 0.599 on the entire dataset. Precision metric indicates that WMF recovers the highest proportion of segmentation in relation to the area identified with an improvement of 0.041 compared to the second best solution (7th). Finally, the systolic PC-MRA applied to the other time frames demonstrates a superior capacity for aorta segmentation compared to the PC-MRA(t) one. Although WMF and the systolic PC-MRA are temporally fixed features, WMF has the ability to better represent areas of blood flow.

Table 1: Results obtained for threshold segmentation on each feature for the complete dataset. **Best** and second best results bold and underlined respectively.

#	Feature	IoU	Dice	Recall	Precision
1	PC-MRA(t)	0.129	0.215	<u>0.596</u>	0.151
2	PC-MRA (sys)	0.205	0.324	0.586	0.250
3	WMF	0.262	0.408	0.569	0.331
3	$\text{Mag}(t) * (1 - \text{WMF})^8$	0.225	0.358	0.564	0.271
4	$\text{Mag}(t)/\text{WMF}$	0.180	0.293	0.584	0.214
5	$\text{Mag}(t)/\text{WMF}^2$	0.224	0.356	0.555	0.275
6	PC-MRA(t)/WMF	0.202	0.324	0.599	0.241
7	PC-MRA(t)/WMF ²	<u>0.237</u>	<u>0.374</u>	0.584	<u>0.290</u>

4 WMF in segmentation task using deep learning

4.1 Method

In order to analyse the contribution of WMF to the deep learning segmentation task, the classical U-Net architecture [14] is used in a 3D configuration, with the time dimension being ignored. The contracting path is constituted by a series of convolution blocks, with each block comprising two convolutions with a kernel size of $3 \times 3 \times 3$. Each convolution is followed by a ReLU activation function. Between each block, a 3D max pooling operation is performed to reduce the resolution size of features with a factor of 2. The expansive path is made of the same blocks than the contracting one. Upsampling features between each block is performed thanks to transposed convolution ("Up-Convolution") using a kernel size of $2 \times 2 \times 2$. A final $1 \times 1 \times 1$ convolution and Sigmoid operation are performed to classify the voxels. U-Net contracting path is made of 4 convolution blocks with, respectively, [64, 128, 256, 512] channels.

The training is performed based on the sum of the Binary Cross Entropy and Dice losses. The network is trained using a combination of different types of image/feature as input. The images and features that have been combined for this task are as follows: Magnitude image (anatomical image, Mag), velocity norm (\mathcal{V}), WMF, PC-MRA(t) and PC-MRA(sys) at the systolic frame. The input images and features are then concatenated before being processed by the network.

Dataset The same dataset has been used for this task as the threshold segmentation, as referenced in Section 3.1. The validation and test sets are each composed of 6 MRIs. Training set is made of 30 MRIs. One of the acquisitions has been removed from the dataset due to incompatibility with the input network dimensions. The selection of images to be incorporated within the test and validation sets was undertaken manually. These sets have been chosen to represent the variety of data (contrast, spike artifacts, acquired planes) by using a stratified sampling method. For the training and validation sets, 10 patches with

Table 2: Results obtained for deep learning segmentation on the test set. **Best** and **second best** results bold and underlined respectively.

#	Input	IoU avg. (std)	median	Dice avg. (std)	median
1	Mag(t)	0.542 (0.107)	0.507	0.697 (0.090)	0.672
2	Mag(t) $\mathcal{V}(t)$	0.513 (0.110)	0.564	0.671 (0.104)	0.721
3	Mag(t) $\mathcal{V}(t)$ WMF	0.671 (0.130)	0.683	<u>0.795</u> (0.104)	0.812
4	Mag(t) $\mathcal{V}(t)$ PC-MRA(t)	0.485 (0.143)	0.504	0.640 (0.138)	0.670
5	Mag(t) $\mathcal{V}(t)$ WMF PC-MRA(t)	<u>0.665</u> (0.086)	0.647	0.796 (0.061)	0.786
6	Mag(t) $\mathcal{V}(t)$ PC-MRA (sys)	0.555 (0.269)	<u>0.674</u>	0.664 (0.288)	<u>0.805</u>
7	Mag(t) $\mathcal{V}(t)$ WMF PC-MRA (sys)	0.625 (0.157)	0.659	0.756 (0.134)	0.795

a size of $48 \times 48 \times 24$ are extracted from each labelled time frame. As 3 time frames are labelled per MRI, the training set is composed of 900 patches and 180 for validation. The test set is made of the selected labelled 4D Flow MRI volumes which represents 18 3D images.

Evaluation and Implementation To evaluate the network, Dice score and IoU are used to estimate the overlap between predicted aorta segmentation and label segmentation. Average and median along the dataset of each metric is given.

The experiment is implemented using Python (v3.12.6) and PyTorch (v2.4.1). The network is trained on a Nvidia A100 80 GB and CUDA (v12.1). The SGD optimizer was used, with a momentum of 0.9 and a weight decay of 10^{-4} . The initial learning rate is set at 0.05, and it undergoes a decrease during the training process as follows: $lr = lr_{\text{initial}} * (1 - epoch_{\text{current}}/epoch_{\text{max}})^{0.9}$.

A set of data augmentation techniques is applied with a probability of 0.5, including random noise, contrast, rotation, and elastic transformation. Random contrast augmentation employs either a random gamma or a random bias field transformation (from the TorchIO library [13]).

4.2 Results

Table 2 presents the performance metrics for the deep learning segmentation task with respect to different feature combinations.

The network achieves better results when it uses the WMF feature as input (as shown by the training #3, 5 and 7). The combination using the peak systolic PC-MRA as input demonstrates optimal outcomes among the non-WMF trainings, attaining the second-best median for both metrics (0.009 and 0.007, IoU and Dice Score, respectively, behind #3). In a low-contrast contexts, segmentation is severely impacted when relying solely on PC-MRA. This is evidenced by the discrepancy between the average and median metrics for training #6, with a difference of 0.119 and 0.141 for the IoU and the Dice Score, respectively. Compared to PC-MRA, WMF shows a minimal disparity between the mean and the median (0.012 and 0.017 for the IoU and Dice Score, respectively), which

indicates a certain contrast robustness. This is attributable to the absence of anatomy in the feature calculation, a factor that renders it significantly more robust to the particularities of the image. This assertion is corroborated by the observation that the presence of WMF in solution #7 has resulted in a substantial reduction in the discrepancy between the means and the medians compared to the combination #6.

5 Discussion

The threshold and deep learning segmentation experiments showed the importance of WMF feature for the segmentation task. The information provided by the hull of pulsatile velocity voxels helps the segmentation task and gives information about the fluid domain over time. Furthermore, during the training process it emerged that the network converged more rapidly toward the optimal solution when using WMF or systolic PC-MRA as input.

PC-MRA is a function of both the anatomy and velocity components. In contrast, WMF is only a function of the velocity itself. Furthermore, the distribution of fluid domain velocity noise is dependent on anatomical SNR [7]. The anatomical and velocity SNR should have an effect on both PC-MRA and WMF. However, an observation of the deep learning test dataset (comprising only six volumes) revealed a reduced sensitivity to the SNR for the proposed feature WMF. This observation requires confirmation using a larger dataset.

Threshold segmentation results indicate that $PC-MRA(t)$ is notably affected by image speed during diastole, corresponding to reduced velocity SNR. A 2.5-fold decrease in the PC-MRA Dice score is observed between peak systole and diastole (0.327 vs. 0.129), whereas WMF values remain stable (0.409 vs. 0.407). WMF, as it incorporates velocity information over several timeframes to characterize pulsatility, exhibits reduced sensitivity to velocity SNR.

During the experiments, combinations of PC-MRA and WMF has been tested and provide interesting results (#7 for threshold segmentation and #5 for deep learning one). PC-MRA and WMF are not opposed to each other, each provides different information. PC-MRA is a handcraft feature that highlights the high anatomy and velocity values in any 4D Flow MRI frame. WMF, on the other hand, represents the hull of all pulsatile velocity voxels. It is a new way to represent 4D Flow MRI images. Besides, it could be used as biomarker in clinical analysis to have a better understanding of the fluid domain and the pulsatility.

6 Conclusion

In this study, a novel handcraft feature, called Weighted Mean Frequencies (WMF), is presented for 4D Flow MRI. WMF has been introduced with the objective of assisting the task in differentiating between pulsatile and non-pulsatile fluid regions. Classical PC-MRA and WMF provide complementary information.

WMF showed the capacity to improve results of 4D Flow MRI segmentation using a threshold or a deep learning approach. This feature helps the network find fluid domains and converge faster during the training phase.

Moreover, deep learning segmentation using WMF as input should be deeper investigated by using more recent approaches as Transformer [6, 15] or Mamba [9, 8]. WMF seems to exhibit a low sensitivity to the velocity SNR. Due to the size of the test dataset, an investigation on a larger clinical dataset should be done with more patients and MRI manufacturers. Finally, WMF could be used as a pulsatility biomarker or a tool to detect fluid domain within low quality 4D Flow MRI.

References

- Berhane, H., Scott, M., Elbaz, M., Jarvis, K., McCarthy, P., Carr, J., Malaisrie, C., Avery, R., Barker, A.J., Robinson, J.D., Rigsby, C.K., Markl, M.: Fully automated 3D aortic segmentation of 4D flow MRI for hemodynamic analysis using deep learning **84**(4), 2204–2218. <https://doi.org/10.1002/mrm.28257>
- Bock, J., Frydrychowicz, A., Stalder, A.F., Bley, T.A., Burkhardt, H., Hennig, J., Markl, M.: 4d phase contrast mri at 3 t: Effect of standard and blood-pool contrast agents on snr, pc-mra, and blood flow visualization. *Magnetic Resonance in Medicine* **63**(2), 330–338 (2010). <https://doi.org/10.1002/mrm.22199>
- Bustamante, M., Viola, F., Engvall, J., Carlhäll, C.J., Ebbers, T.: Automatic time-resolved cardiovascular segmentation of 4D flow MRI using deep learning. *J. of Magn. Reson. Imaging* **57**(1), 191–203 (2023). <https://doi.org/10.1002/jmri.28221>
- Bustamante, M., Gupta, V., Forsberg, D., Carlhäll, C.J., Engvall, J., Ebbers, T.: Automated multi-atlas segmentation of cardiac 4d flow mri **49**, 128–140 (2018). <https://doi.org/10.1016/j.media.2018.08.003>
- Dumoulin, C.L., Souza, S.P., Walker, M.F., Wagle, W.: Three-dimensional phase contrast angiography. *Magnetic Resonance in Medicine* **9**(1), 139–149 (1989). <https://doi.org/10.1002/mrm.1910090117>
- Hatamizadeh, A., Tang, Y., Nath, V., Yang, D., Myronenko, A., Landman, B., Roth, H.R., Xu, D.: Unetr: Transformers for 3d medical image segmentation. In: 2022 IEEE/CVF Winter Conference on Applications of Computer Vision (WACV). pp. 1748–1758 (2022). <https://doi.org/10.1109/WACV51458.2022.00181>
- Levilly, S., Castagna, M., Idier, J., Bonnefoy, F., Le Touzé, D., Moussaoui, S., Paul-Gilloteaux, P., Serfaty, J.: Towards quantitative evaluation of wall shear stress from 4D flow imaging **74**, 232–243 (2020). <https://doi.org/10.1016/j.mri.2020.08.017>
- Liao, W., Zhu, Y., Wang, X., Pan, C., Wang, Y., Ma, L.: Lightm-unet: Mamba assists in lightweight unet for medical image segmentation (2024). <https://doi.org/10.48550/arXiv.2403.05246>
- Ma, J., Li, F., Wang, B.: U-mamba: Enhancing long-range dependency for biomedical image segmentation. *arXiv preprint arXiv:2401.04722* (2024)
- Marin-Castrillon, D.M., Lalande, A., Leclerc, S., Ambarki, K., Morgant, M.C., Cochet, A., Lin, S., Bouchot, O., Boucher, A., Presles, B.: 4D segmentation of the thoracic aorta from 4D flow mri using deep learning. *Magnetic Resonance Imaging* **99**, 20–25 (2023). <https://doi.org/10.1016/j.mri.2022.12.021>
- Markl, M., Frydrychowicz, A., Kozerke, S., Hope, M., Wieben, O.: 4D Flow MRI. *J. Magn. Reson. Imaging* **36**(5), 1015–1036 (2012). <https://doi.org/10.1002/jmri.23556>, <http://dx.doi.org/10.1002/jmri.23556>

12. Pelc, N.J., Bernstein, M.A., Shimakawa, A., Glover, G.H.: Encoding strategies for three-direction phase-contrast MR imaging of flow. *J. Magn. Reson. Imaging* **1**(4), 405–413 (1991). <https://doi.org/10.1002/jmri.1880010404>, <http://dx.doi.org/10.1002/jmri.1880010404>
13. Pérez-García, F., Sparks, R., Ourselin, S.: TorchIO: A Python library for efficient loading, preprocessing, augmentation and patch-based sampling of medical images in deep learning **208**, 106236. <https://doi.org/10.1016/j.cmpb.2021.106236>
14. Ronneberger, O., Fischer, P., Brox, T.: U-net: Convolutional networks for biomedical image segmentation. In: Navab, N., Hornegger, J., Wells, W.M., Frangi, A.F. (eds.) *Medical Image Computing and Computer-Assisted Intervention – MICCAI 2015*. pp. 234–241. Springer International Publishing, Cham (2015). https://doi.org/10.1007/978-3-319-24574-4_28
15. Shaker, A., Maaz, M., Rasheed, H., Khan, S., Yang, M.H., Shahbaz Khan, F.: Unetr++: Delving into efficient and accurate 3d medical image segmentation. *IEEE Transactions on Medical Imaging* **43**(9), 3377–3390 (2024). <https://doi.org/10.1109/TMI.2024.3398728>
16. Yushkevich, P.A., Piven, J., Cody Hazlett, H., Gimpel Smith, R., Ho, S., Gee, J.C., Gerig, G.: User-guided 3D active contour segmentation of anatomical structures: Significantly improved efficiency and reliability. *Neuroimage* **31**(3), 1116–1128 (2006). <https://doi.org/10.1016/j.neuroimage.2006.01.015>